②

AD-A233 123	PAGE	Form Approved OMB No. 0704-0188

Public reporting gathering and n this collection o Davis Highway,

...per response, including the time for reviewing instructions, searching existing data sources, ...tion of Information. Send comments regarding this burden estimate or any other aspect of ...tion Headquarters Services, Directorate for Information Operations and Reports, 1215 Jefferson ...nt and Budget, Paperwork Reduction Project (0704-0188), Washington, DC 20503.

1. Agency Use Only *(Leave blank).*	2. Report Date. 1991	3. Report Type and Dates Covered. Journal Article

4. Title and Subtitle.
The Role of the Microstructure of Pacific Red Clays in Radioactive Waste Disposal

6. Author(s).
Patti J. Burkett, Richard H. Bennett, and William R. Bryant

5. Funding Numbers.
Program Element No. 61153N
Project No. 03205
Task No. 330
Accession No. DN257003

7. Performing Organization Name(s) and Address(es).
Naval Oceanographic and Atmospheric Research Laboratory*
Ocean Science Directorate
Stennis Space Center, MS 39529-5004

8. Performing Organization Report Number.
JA 360:036:89

9. Sponsoring/Monitoring Agency Name(s) and Address(es).
Naval Oceanographic and Atmospheric Research Laboratory*
Ocean Science Directorate
Stennis Space Center, MS 39529-5004

10. Sponsoring/Monitoring Agency Report Number.
JA 360:036:89

11. Supplementary Notes.
*Formerly Naval Ocean Research and Development Activity
MFGS

DTIC ELECTE APR 02 1991 S G D

12a. Distribution/Availability Statement.

Approved for public release; distribution is unlimited.

12b. Distribution Code.

13. Abstract *(Maximum 200 words).*
The objective of this study was to examine the microfabric of red clay sediments from the Central Pacific deep-sea basin using transmission electron microscopy by assessing the response of the fabric to thermal and mechanical influences resulting from the testing of simulated radioactive waste. The affected samples analyzed were cored from remolded, laboratory consolidated, illitic-rich red clay used in the In Situ Heat Transfer Experiment Simulation test (ISIMU) (Percival, 1982). The fabric of these samples was compared to models, and to undisturbed samples designated RAMA, obtained from gravity cores at the MPG-1 site located in the Central Pacific Ocean. Specific objectives of this study included an analysis of the microfabric characteristics as a result of (1) mechanical disturbances from sediment remolding and heater probe insertion (2) heating of the sediment causing induced thermal gradients, and (3) comparison of the "undisturbed" red clays to the remolded material. In addition we studied the changes in the physical properties, such as undrained shear strength, water content, void ratio, and mineralogy as they related to the microfabric.

14. Subject Terms.
(U) Sediment Transport; (U) Sediments; (U) Pore Pressure; (U) Clay

15. Number of Pages. 19

16. Price Code.

17. Security Classification of Report. Unclassified	18. Security Classification of This Page. Unclassified	19. Security Classification of Abstract. Unclassified	20. Limitation of Abstract. SAR

Reprinted from

Richard H. Bennett, William R. Bryant, and Matthew H. Hulbert
Editors

Microstructure of Fine-Grained Sediments

CHAPTER 52

The Role of the Microstructure of Pacific Red Clays in Radioactive Waste Disposal

Patti J. Burkett, Richard H. Bennett, and William R. Bryant

Introduction

The objective of this study was to examine the microfabric of red clay sediments from the Central Pacific deep-sea basin using transmission electron microscopy by assessing the response of the fabric to thermal and mechanical influences resulting from the testing of simulated radioactive waste. The affected samples analyzed were cored from remolded, laboratory consolidated, illitic-rich red clay used in the *In Situ* Heat Transfer Experiment Simulation test (ISIMU) (Percival, 1982). The fabric of these samples was compared to models, and to undisturbed samples designated RAMA, obtained from gravity cores at the MPG-1 site located in the Central Pacific Ocean. Specific objectives of this study included an analysis of the microfabric characteristics as a result of (1) mechanical disturbances from sediment remolding and heater probe insertion, (2) heating of the sediment causing induced thermal gradients, and (3) comparison of the "undisturbed" red clays to the remolded material. In addition we studied the changes in the physical properties, such as undrained shear strength, water content, void ratio, and mineralogy as they relate to the microfabric.

Background

The objectives of the Subseabed Disposal Program (SDP) were to evaluate the feasibility of disposing of high-level radioactive waste within fine-grained sediments of the world ocean basins by carefully designed emplacement methods, and to design and evaluate the technology required for the feasibility of subseabed disposal (Hollister et al., 1981; Percival, 1983; Percival et al., 1987). This concept is not to be confused with dumping of waste into the water column (prohibited by Article IV 1a of the London Dumping Convention, 1978), or placement of waste on the sea floor. The SDP criterion for possible nuclear waste disposal considers four major factors. First, the site should be tectonically stable including no erosional evidence and minimal recent faulting. Second, the geologic processes and changes must be reasonably predictable within the same time scale as the rate of radionuclide decay, i.e., millions of years, and regionally uniform both horizontally and vertically. A third significant qualifier is the remoteness of available natural resources resulting in a marine "desert" with restricted biological activity and few mineral resources. Finally, man's activities and harmful climate effects must be distant from the site.

In accordance with established SDP criteria, the selected MPG-1 (mid-Pacific lithospheric plate, mid-gyre between the great currents) study area was located approximately 600 miles north of Hawaii in the Central North Pacific Ocean between the Mendocino and Murray Fracture Zones (Hollister, 1977). The sediment, collected in a water depth of 5705 m, is composed of cohesive, chocolate brown colored, predominantly clay-size particles referred to as abyssal red clays (Bryant and Bennett, 1988). They are composed of authigenic materials, windblown particles, and volcanic and insoluble biogenic debris.

The *In Situ* Heat Transfer Experiment (ISHTE) is a phase of SDP and the objectives are to provide data on the *in situ* thermal, fluid dynamic, thermochemical, and mechanical sediment responses to the emplacement of radioactive waste in the seabed. Measurements of the thermal response of the sediment were compared with numerical predictions to validate a thermomechanical model for deep-sea sediments (Olsen and Harrison, 1979; Percival et al., 1980). An integral part of ISHTE is the development and demonstration of the technology required to perform waste isolation experiments in the seabed in water depths of 6000 m (Percival et al., 1980, 1987). A scaled laboratory
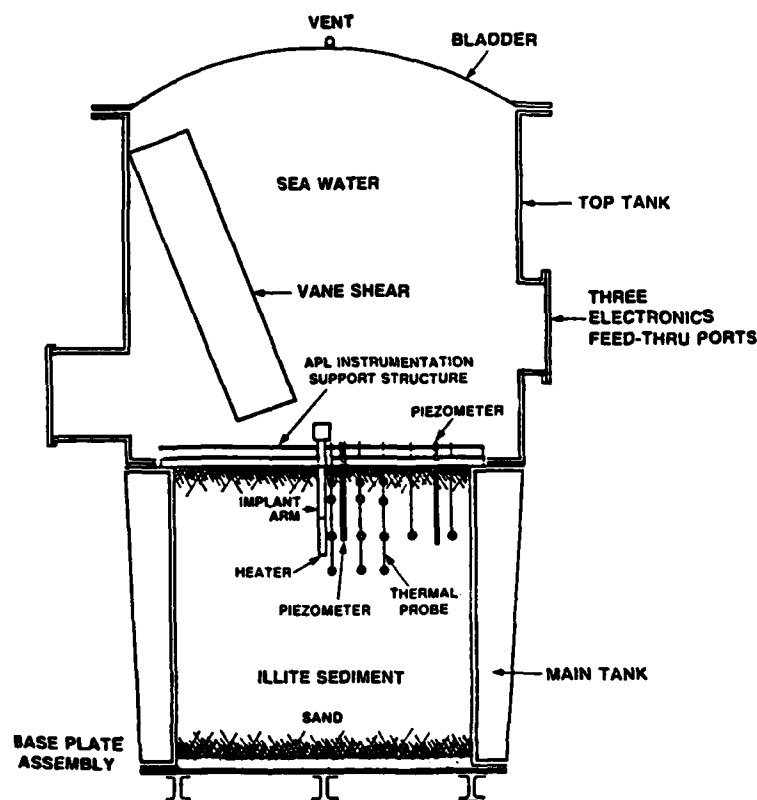
Figure 52.1. ISIMU test tank setup with reconstituted illitic sediment subjected to equivalent deep-sea ambient pressure in a hyperbaric chamber. (Redrafted from Silva and Jordan, 1983.)

ISHTE Simulation experiment (ISIMU) was conducted in 1981 by Sandia National Laboratories and participating institutions (Percival, 1982). ISIMU was designed to simulate predicted environmental field conditions and to test some of the instruments of a full-scale ISHTE experiment. The test was performed in a 1-m³ cylindrical container filled with remolded, laboratory consolidated, illitic red clay recovered by dredged hauls from the proposed ISHTE test site (Fig. 52.1) (Silva and Jordan, 1984). ISIMU was conducted in a hyperbaric chamber at the David Taylor Naval Ship Research and Development Center, Annapolis, Maryland. A calculated scale of approximately 0.28:1.0 allowed adequate thermal equilibrium to be reached within 1 month. The dredged sediment was reconstituted in a rotary mixer with 34.2 ppt salinity seawater until a homogeneous slurry was formed. A series of thin (approximately 20 cm thick) layers of the slurry was added to the tank, and a vacuum was applied to each layer to remove excess air. Consolidation, occurring over a 10-week period, simulated in situ porosities of the deep ocean sediments (Silva and Jordan, 1983). The tank, sediments, and emplaced instrumentation were pressurized to 55 MPa at 4°C and the experiment was run for 1 month. After cool down, the heater probe was overcored and a second core adjacent was collected. The 12 fabric subsamples used in this analysis were collected normal to the longitudinal axis of the two cores at selected distances from the heater's edge and at mea-

sured depths below the mudline (Fig. 52.2). The RAMA control samples were subcored from undisturbed gravity core samples obtained from the MPG-1 site.

Methods

Grain-Size Determination

A remolded, laboratory-consolidated sample remote from the heater probe and a RAMA control sample were analyzed for grain size using Micromeritics Model 5000 particles size analyzer for the 4ϕ to 10ϕ (ϕ = negative log to the base 2 of the size in mm) silt and clay-size fractions. The calculations and resultant graph of cumulative percent versus phi distribution (ϕ) utilizes the principle of Stokes' law. The statistical data including the mean phi, standard deviation, skewness, kurtosis, and normalized kurtosis were calculated according to Folk and Ward (1957) for analysis and validation of the data in comparison to conventional data.

X-ray Diffraction

X-ray diffraction (XRD) was performed using techniques modified from Jackson (1969). Carbonates, organic matter, man-

Figure 52.2. Diagram showing position of ISIMU heater probe in relationship to piston cores 1 and 2, and the subsamples used for clay microfabric analysis.
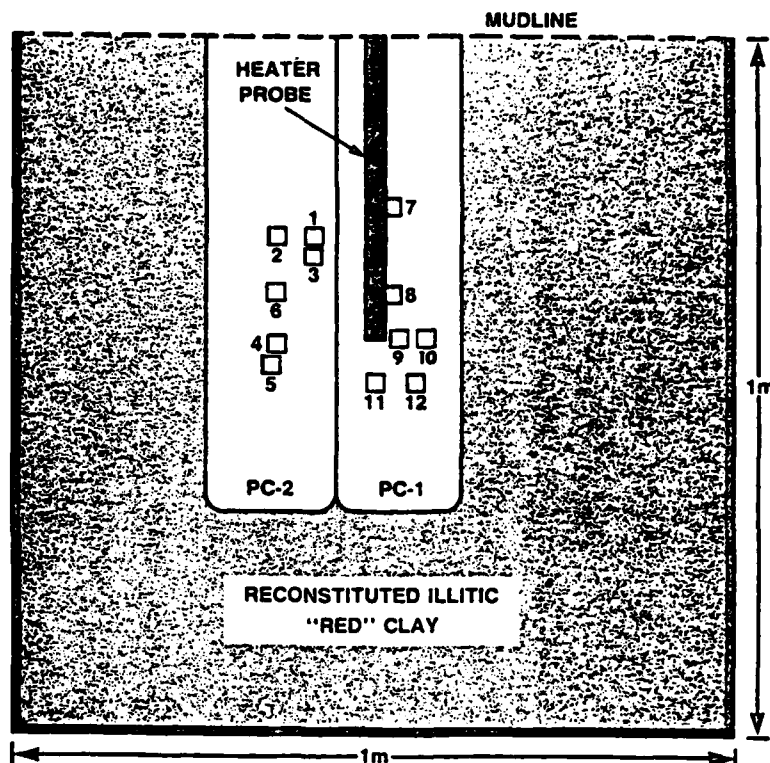
ganese dioxide, and free iron were removed. This was necessary since they act as binding agents, inhibit dispersion, and thus interfere with fractionation for mineral identification. Fractionation was accomplished by optimizing the pH, centrifuging with pH 10 Na^2CO^3 and flocculating in 1 N NaCl. The samples were saturated with magnesium and potassium. Oriented specimens were prepared by air drying a slurry of the clay on a glass slide. Vicor glass was used for the heated samples. The Mg^{2+} saturated samples were X-rayed at 25°C (room temperature), then glycerol solvated, and X-rayed again. The K^+ saturated sample slide was X-rayed following heat treatment of 25, 330, and 550°C.

Selected Area Diffraction

X-ray diffraction and selected area diffraction (SAD) analysis can provide information on lattice parameters and crystal symmetry of a mineral. SAD uses an aperture located in the column of the TEM to block all diffraction patterns except those obtained in a very small selected area of the specimen (Veblen, 1986). Different orientations of crystals can be recorded on SAD patterns, and varying intensities also can provide structural information. The mineral, illite, a phyllosilicate whose polycrystals yield a distinct ring pattern with varying diameters, was compared with the powder diffraction file d-spacings (distance

between the crystal lattice comprised of periodic parallel planes of atoms) (ASTM Index, 1969), matching Miller indices and thus identifying the mineral species (Andrews et al., 1971).

Rose Diagram Orientation

Fabric orientation analysis was performed using a Rose diagram and frequency histogram. The direction of elongation of the particles and domains was measured from the micrographs in reference to an arbitrary straight line, in 10° increments from 0° to 180°. The particles measured were categorized by size. More than 1000 particles and small domains < 1 μm, and more than 300 elongated domains ≥ 1-5 μm, were examined. The resulting plot from the measured orientations, the Rose diagram, and frequency histogram provided a data base for comparison between samples. The frequency histogram was derived by calculating the percentage of particles in 10° increments from the total count and plotting frequency (%) versus degree (°).

Microfabric Sample Preparation

The sample preparation of fine-grain illitic-rich clay sediment used for the TEM microfabric analysis employed the methods first described by Bennett (1976). A detailed description of the
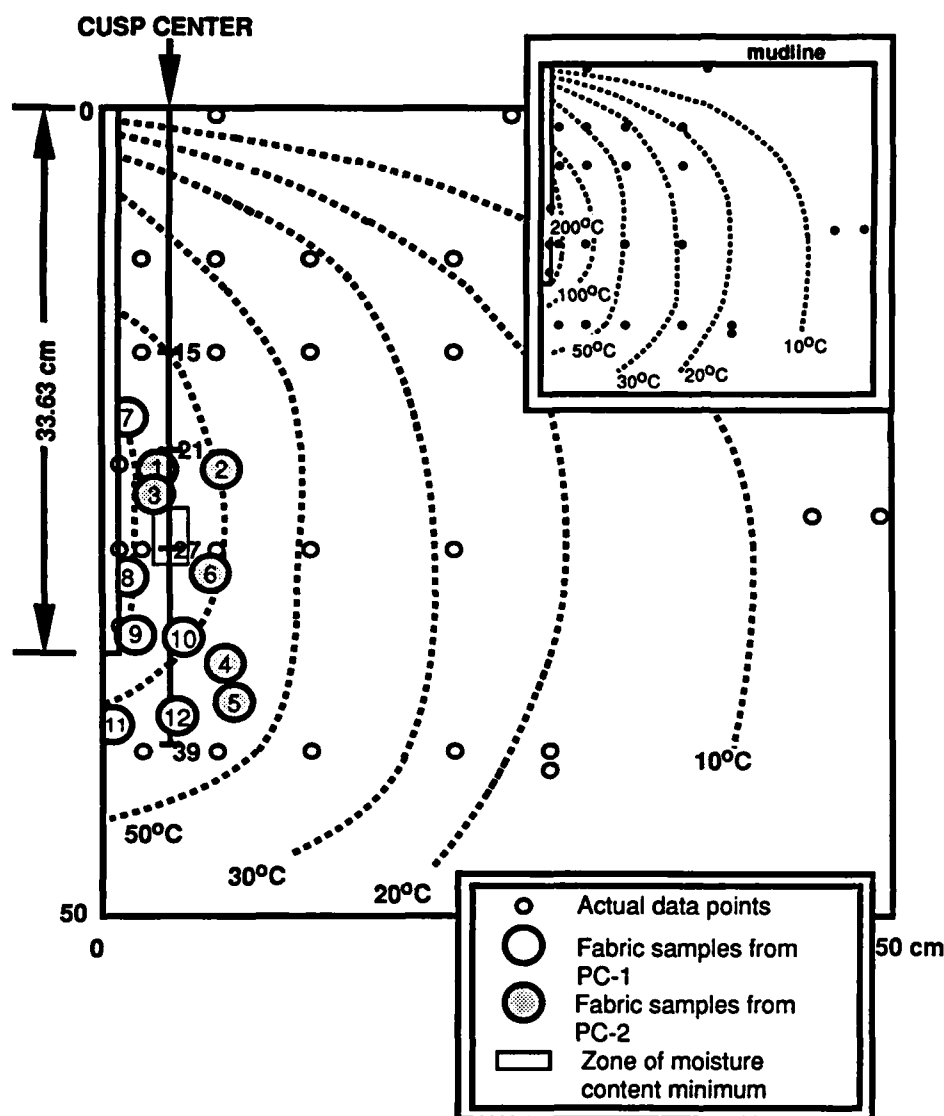
Figure 52.3. Steady state isotherm (drafted by H. Li, interpolated from experimental data, Miller et al., 1982) showing position of 12 microfabric samples, and the cusp samples used for X-ray diffraction analysis.

techniques is presented in this volume by Baerwald, Burkett, and Bennett. Micrographs using TEM were taken at magnifications of 8000× and 16,000×.

Results and Discussion

Thermal Effects

The significant effects resulting from this analysis as a result from thermal exposure include (1) mineral transformation, (2) physical properties alterations, and (3) diagnostic microfabric features observed in TEM.

The steady-state isotherm diagram (Fig. 52.3) shows the thermal fields generated by the heater probe for a total power dissi-

pation of 160 W. The highest temperature generated, 296°C, occurred in a narrow region surrounding the lower 15 cm of the heater probe. Fabric sample B-8 originated from the highest intensity thermal zone, 200–296°C. Rapid decreases in temperatures were recorded radially away from the heater. Locations of the fabric samples relative to the distance from the heater edge and to the mudline depth are found in Table 52.1. Fabric samples B-1, B-3, B-7, and B-9 fell within the 100–200°C isotherm. Samples B-2, B-6, and B-10 were located proximal to the 100°C isotherm. Fabric samples B-4, B-5, B-11, and B-12 were exposed to temperatures within the 50–100°C zone.

The water content (expressed as percent dry weight) of the sediment from the cusp between cores PC-1, PC-2, and PC-3 varies with sediment depth. Figure 52.4 illustrates the 10% reduction (102% to 92%) in water content from 8 to 33 cm below

Table 52.1. ISIMU fabric samples by identification number, core number, distance from the edge of the heater, and depth below mudline.

Sample number	Core number	Depth below mudline (cm)	Distance from heater edge (cm)
B-1	PC-2	21.4–22.9	1.5
B-2	PC-2	21.4–22.9	5.5
B-3	PC-2	23.1–24.6	1.5
B-4	PC-2	33.4–34.9	5.5
B-5	PC-2	35.9–37.4	6.0
B-6	PC-2	27.5–28.0	5.5
B-7	PC-1	18.1–19.6	0.0
B-8	PC-1	27.8–29.3	0.0
B-9	PC-1	32.8–34.3	0.5
B-10	PC-1	32.8–34.3	3.5
B-11	PC-1	37.3–38.8	Directly under heater
B-12	PC-1	37.3–38.8	2.5

the sediment surface (mudline). Beyond the end of the probe at 33 cm, the water content increased slightly less than 10%, which is close to the value at 8 cm. Baking, in the ISIMU experiment (assuming 100% saturation of the sediment), is followed by consolidation of sediments, loss of pore fluid, and an accompanying decrease in void ratio. Radially, water contents are low between 2 and 4.7 cm, including the cusp zone created between cores 1, 2, and 3. Beyond approximately 5 cm, the water content fluctuates. The grided area of Figure 52.4 represents the zone of minimum water contents. No fabric samples were collected from this zone, but assuming axial symmetry of the thermal gradients (100–200°C), sediment of samples B-1, B-3, B-9, and B-10 probably experienced the same thermal effects from heating as the grided zone. The significant decrease in the water content near the heat source may have resulted from induced thermal effects resulting in pore water diffusion, consolidation, and chemical reaction.

The undrained shear strength profiles are depicted for three vertical test sequences: pretest unheated, heated, and post-test cooled conditions (Silva and Jordan, 1984 and Fig. 52.5). The large shear strength increase between 20 and 32 cm sediment depth during heating corresponds directly to the water content decrease (Fig. 52.4). The 38 kPa (375 g/cm²) shear strength maximum, occurring at 170°C corresponds to the 33 cm depth at the end of the heater probe and probably results from localized dewatering as a result of heating. The comparison of the maximum shear strength profile during heating and the profile obtained before heating indicates a 10-fold increase in shear strength. At the termination of the test (after cool-down), the sediment shear strength appears to have decreased, but not back to its original pretest strengths. This implies a slight thermally reversible or a residual characteristic strength following cool-down of this sediment type.

Samples located at various depths approximately 3.5 cm from the heater centerline in the cusp between cores PC-1, PC-2, and PC-3 were analyzed for clay mineralogy (Fig. 52.6). At a depth
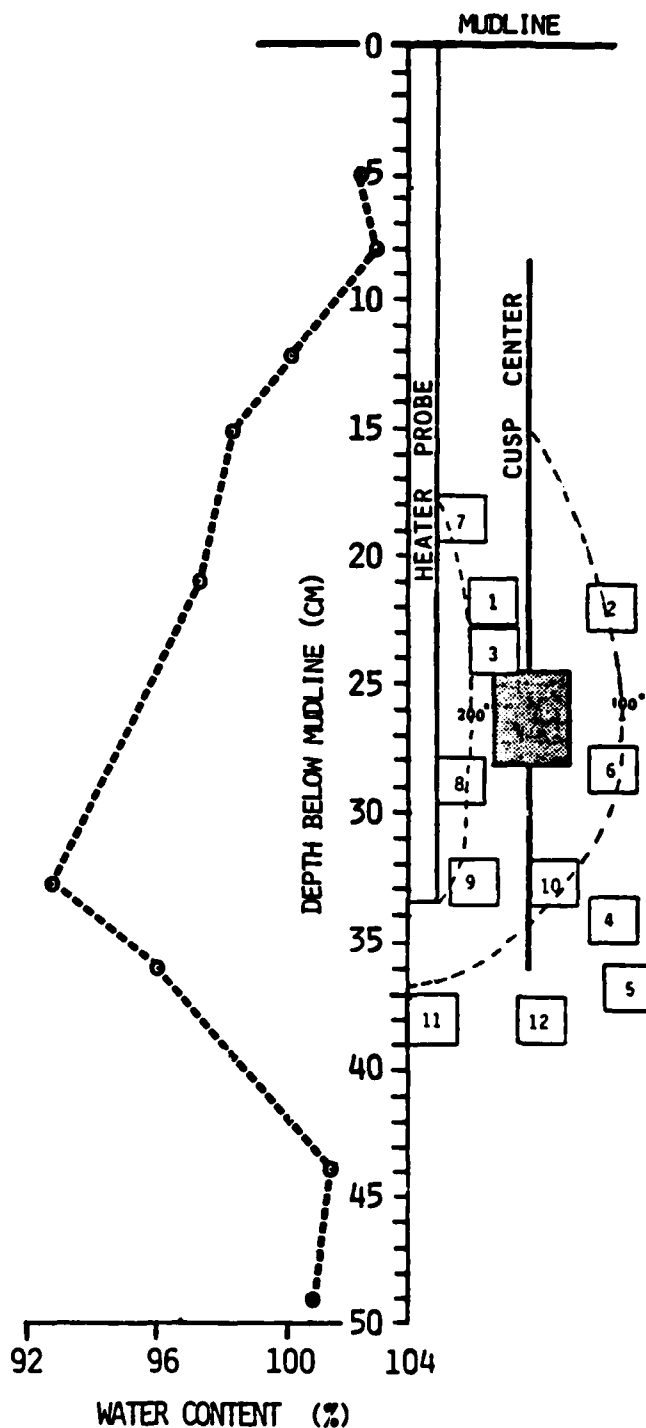
Figure 52.4. Water content versus cm depth profile for ISIMU post-test samples showing water content minimum corresponding to the end of the heater probe.

of 7 cm, the sediment was comprised of approximately 5% smectite, 34% chlorite, 48% illite, and 13% kaolinite. At 24 cm the mineral composition changed to 40% smectite, 20% chlorite, 40% illite, and trace amounts (less than 5%) of kaolinite. After

UNDRAINED SHEAR STRENGTH, S_u (g/cm²)

DEPTH, D (cm) FROM BOTTOM OF EHS STRUCTURE

O—O PRETEST UNHEATED
(19-21 cm FROM HEATER C.L.
□—□ HEATED
(2.5-6.5 cm FROM HEATER C.L.
△—△ POST-TEST COOLED
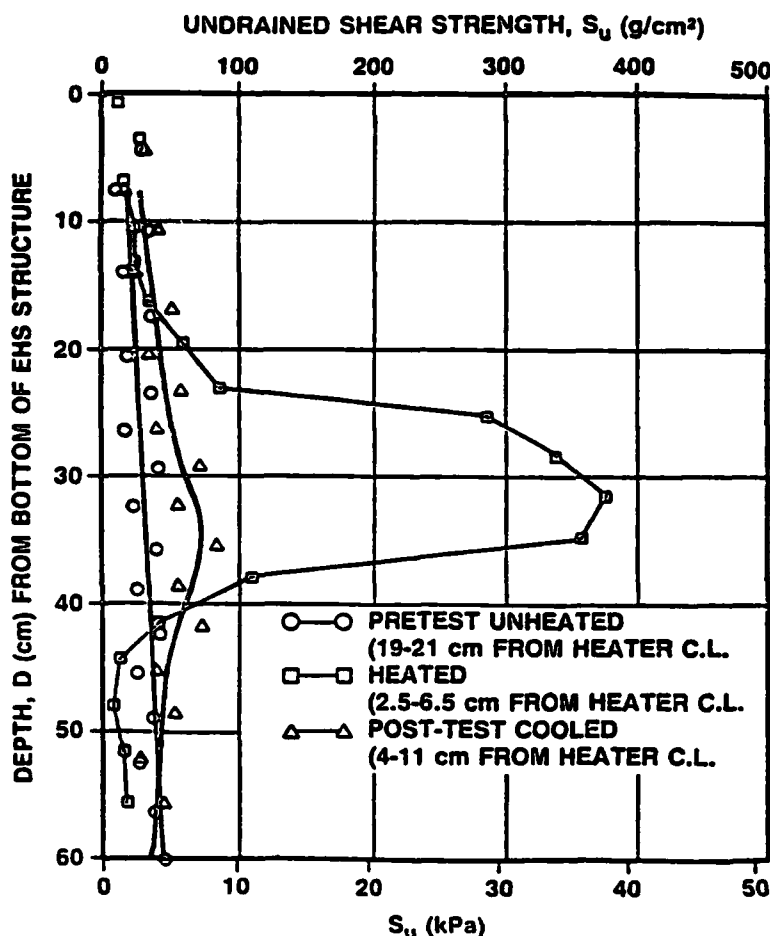(4-11 cm FROM HEATER C.L.

S_u (kPa)

Figure 52.5. ISHTE simulation combined profile. Note the substantial increase in shear strength associated with the heated zone. (Redrafted from Silva and Jordan, 1983.)

consideration of the limits of instruments detection (at least 5% of a mineral in question is necessary for confirmation) and possible errors in calculation, a significant smectite increase accompanied by a change in color from brown to gray is evident. The 7 cm depth is associated with a thermal gradient between 50 and 100°C and water content of 103% (Fig. 52.3). At 24 cm the temperature recorded during the experiment increased to 170°C, with an associated post-test water content of 97% (Fig. 52.4). The water content is a measure of the intergranular pore water and free water or interlayer water not strongly attracted to the mineral skeleton. Routine water content determination procedure dries the sample in a 105°C oven (Lambe, 1951). Greater temperatures remove more of the loosely bonded water, although temperatures of approximately 500°C are required to remove the adsorbed water layer of smectite, therefore collapsing its structure. The detection of increased quantities of smectite is observed by an increase in the peak height on the X-ray patterns. This was evident in the cusp sample at 24 cm (Fig. 52.6). Thorton (1983) studied the transition of a sediment's mineralogy from mixed smectite–illite to an increase in smectite and decrease in mixed-layer clays, after being maintained in a

200–300°C hydrothermal apparatus. Other laboratory syntheses of smectite at elevated temperatures and pressures were carried out by Noll (1930), Sedletski (1937), Harward and Brindley (1964), and Seyfried and Bischoff (1981). Potassium is the cation associated with illite, which binds successive layers. From chemical analysis of the pore fluids, an increase in potassium level was detected in an area adjacent to the cusp. A thermally induced release of interstitial potassium may have resulted in the transformation to smectite, although other geochemical processes and other minerals may have played a role in smectite formation.

Orientation of particles was studied by examining the micrographs of samples B-4, B-5, and B-7 compared to the RAMA samples for possible thermal heating and/or mechanical remolding effects of the sediment (see Table 52.1 for exact location relative to the induced thermal fields generated). Because RAMA was not subjected to the heat source, its ambient *in situ* temperature would have been approximately 4°C.

Analysis of more than 1000 particle measurements on the RAMA mosaic, showing an area of approximately 2500 μm² (Fig. 52.7), revealed a random arrangement of particles (Fig.

52.8) as seen in the histogram and Rose diagram. From similar analysis of samples B-7 (nearfield), B-4 (far-field), B-5 (far-field) has the strongest degree of preferred orientation demonstrated by its Rose diagram and frequency histogram but was subjected to less heat (for further details see Burkett, 1987). Thus particle orientation appears to be independent of sample location relative to the generated thermal gradient determined from orientation analysis. Additional analysis of remolded, non-heated fabric is needed to evaluate the dominant parameter causing particle alignment, heating, or remolding or both. If the remolded samples do demonstrate preference of particle alignment, as indicated from the individual micrographs, perhaps the movement of pore fluids could be sufficient to move particles or small domains to a preferred orientation. Consolidation, the decrease in volume of the sediment resulting from the loss of pore fluid, is an expected outcome from exposure to intense heat. The flow of water originating in the "baked" zone could have affected the samples in the cooler zones. The processes of consolidation and fluid transport during ISIMU have been thoroughly documented analytically by McTigue et al. (1986).

Mechanical Disturbance

Mechanical disturbances of the sediment includes effects from probe insertion and remolding. (Detailed analysis and discussion of laboratory consolidation procedures are found in Bryant and Bennett, 1988.) Remolding can be considered in terms of primary remolding during preparation of the red clay sediment before emplacement in the ISIMU test tank (Fig. 52.1), and a secondary or localized remolding from heater probe penetration into the prepared consolidated sediment. Clay fabric disturbance, as a consequence of probe insertion, is difficult to assess using TEM micrographs. Extreme care was taken when selecting fabric subsamples to avoid any obvious preexisting physical disturbances such as fractures or microcracks in the sediment. The fabric samples were collected near the end of the probe at depths of ~21 to ~38 cm, therefore surface deformation effects of insertion are not considered. Little difference in traction stresses on probe insertion was found with varying textures (0.13–2.16 μm) of the Inconel probe's surface (Silva and Jordan, 1984). A 2 μm surface texture finish for the Inconel probe was chosen to provide good adhesion (forming a good seal) between the heater and remolded sediment, thus preventing water migration along the heater wall. Post-ISIMU, the heater was overcored, the core liner cut, then the sediment was sliced normal to the probe for sampling. If the probe had been extracted, suction forces may have been sufficient to result in large localized sediment deformation. Only fabric samples B-7 and B-8, adjacent to the probe, were expected to show any effect from traction force during insertion. Samples B-7 and B-8 are closest to the heater wall (Fig. 52.2) and generally would be expected to exhibit the most obvious signs of deformation from probe insertion. The fabric subsamples were extracted from the
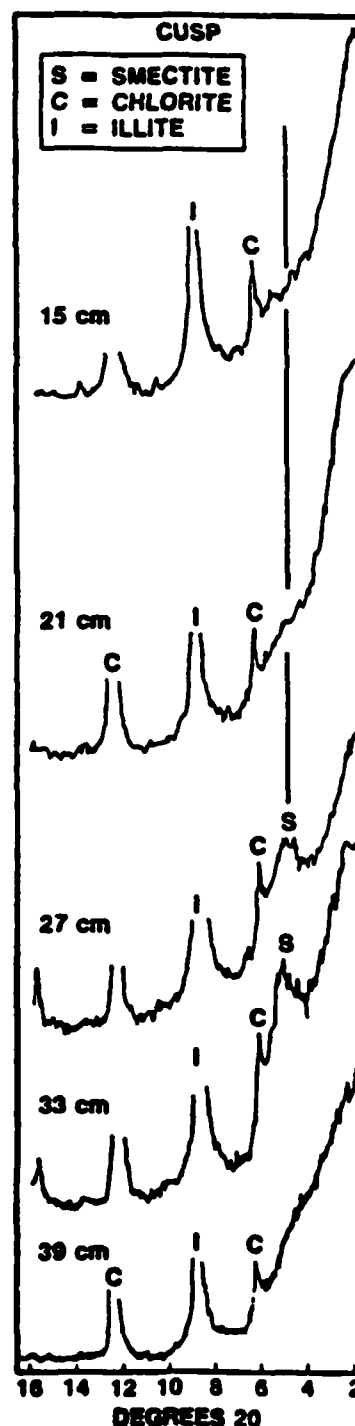

Figure 52.6. X-Ray diffraction pattern showing pronounced increase in the smectite peak occurring at the 27 cm and 33 cm depths.

central portion of the larger samples, and those samples in the plastic zone would be expected to have characteristics such as smearing of the probe–sediment interface and possibly some lateral deformation from probe insertion.

Figure 52.7. Mosaic of the RAMA undisturbed illitic-rich Pacific red clay sediment showing complex assemblage of particles comprising the *in situ* microfabric. Some features include a channel (CH) for transport of pore fluids, fractured illite argillites (F), high void ratio smectitic aggregates (S), denser aggregates (AA), and matrix of ≤ 1 μm domains and small particle (1 μm bar scale in upper left).

Figure 52.8. Rose diagram (A) and frequency histogram (B) for RAMA mosaic showing a completely random distribution of particle arrangements. The dark areas represent 2–5 μm domains, and the lighter areas represent ≤ 1 μm small particles and domains.

A.

B.
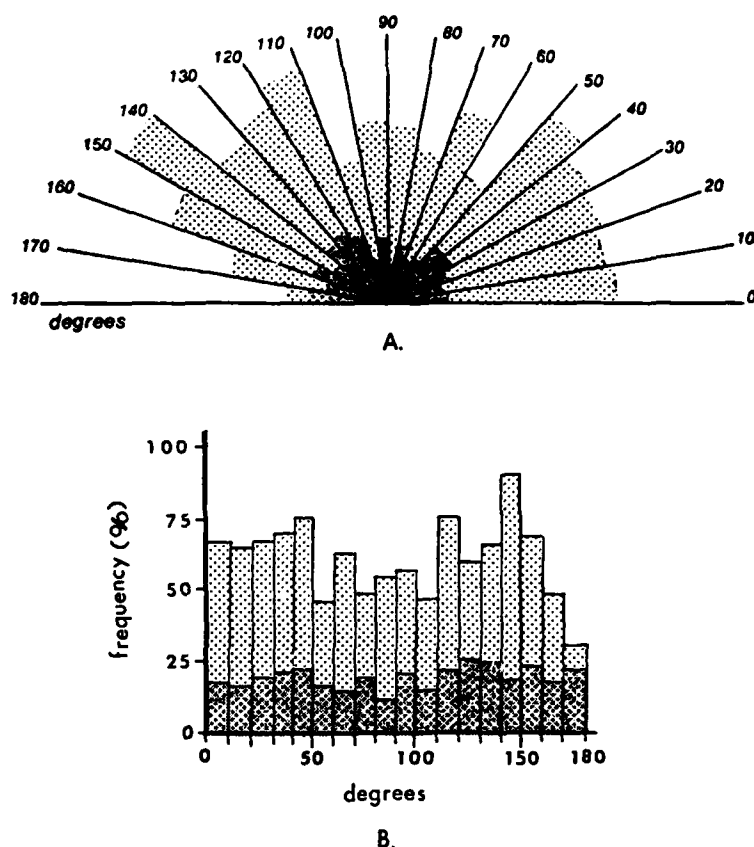
Primary remolding from mechanical disturbances occurs as the illitic-rich dredged sediment is reconstituted and then churned in a cement mixer before consolidation to *in situ* overburden pressures. The expected results from remolding would be breakage, swirling, or bending of long chains of particles or elongated domains and collapse and breakage of fragile flocs and aggregates. These effects would be more pronounced on longer particles than on individual particles or subrounded dense aggregates. If significant, primary remolding effects should be evident in all cores, without regard to the location in reference to the heat source.

Grain size analysis was performed on two samples. RAMA represented the control and core PC-5 was used to assess the effects of reconstituting and laboratory remolding of sediment for experimental purposes. Core PC-5 represented a far-field sample, and was located well beyond the effects from intense heat such as a decrease in water content or an increase in shear strength. The grain size determination resulted in a striking similarity between the two samples (Fig. 52.9). They were both homogeneous (well sorted) with only trace amounts of sand (greater than 4φ). The predominate particles were clay-size (≤3.9 μm) and comprised ~90% of the sample. The silt content of both samples was ~10%, and the remaining portions consisted of sand. These results imply negligible effects on the clay-size particles from

reworking of the illitic-rich pelagic sediment. For all practical purposes the two samples analyzed are nearly identical.

Microfabric Analysis

The major mineral constituent was identified using selected area diffraction techniques. The analysis was performed by comparing polycrystal patterns to an ASTM standard and revealed the presence of the clay mineral illite. Figure 52.10 shows the measured, calculated parameters and percentage differences between the ASTM file values of *d*-spacings and the measured ring diameters of the unknown. The two values range from 0.8 to 6.0% deviation. The *hkl* values can then be assigned to the respective ring. Although polycrystals, suitable for good SAD patterns, located within the mixed assemblage of the *in situ* fabric are not common, many similar and fractured crystals are prevalent. This is significant because illite, the most abundant mineral as determined by X-ray diffraction analysis, now can be positively identified mineralogically and morphologically on the microscale. The identification of individual clay-size particles from mixed mineral assemblages can provide a better understanding of the microstructure and its physicochemical forces that control the sediment's behavior and response to static and dynamic loads.
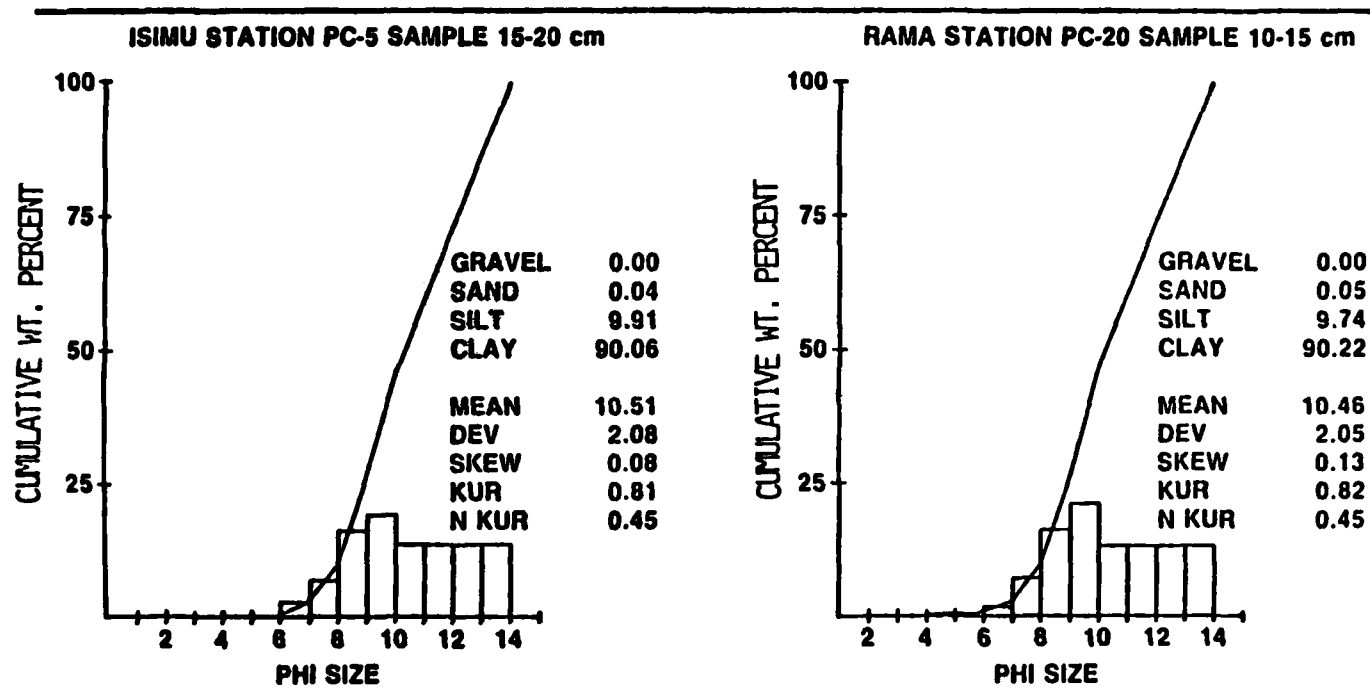
ISIMU STATION PC-5 SAMPLE 15-20 cm

GRAVEL	0.00
SAND	0.04
SILT	9.91
CLAY	90.06
MEAN	10.51
DEV	2.08
SKEW	0.08
KUR	0.81
N KUR	0.45

RAMA STATION PC-20 SAMPLE 10-15 cm

GRAVEL	0.00
SAND	0.05
SILT	9.74
CLAY	90.22
MEAN	10.46
DEV	2.05
SKEW	0.13
KUR	0.82
N KUR	0.45

Figure 52.9. Grain size comparison of RAMA sample to sample PC-5, remolded and laboratory consolidated to equivalent *in situ* porosity. Notice the striking similarity of the grain sizes.

The sediment response from the ISIMU experiment was evaluated by examining TEM micrographs of the 12 fabric samples from ISIMU cores PC-1 and PC-2. Evidence of disturbance from probe insertion was seen in near-field fabric samples B-7 and B-8 adjacent to the heater wall. Sample B-8 shows a slightly denser arrangement of particles than far-field samples such as B-5 (Fig. 52.11A). The fabric has the appearance of broad bands between which are long zones of oriented small domains. These appear to be compression features resulting from probe insertion, and look like microfractures, slip planes, or shear planes. Figure 52.11B, of sample B-11 located under the probe, is an enlargement of the localized oriented chains, predominantly face-to-face, forming a band about 0.5 µm across. Figure 52.11C demonstrates how the shear planes become aligned with chains of oriented domains. The microfracture sample of Figure 52.12A (sample B-8) is subtle because of the lack of separation between the slip planes, but demonstrates the zone of locally oriented particles. Figure 52.12B shows evidence of disturbance as seen by the gap lined with oriented particles. Notice the bent domains, possibly from shearing with planes containing obstacles consisting of larger, subrounded argillites (aeolian shale domains fractured during ultrathin sectioning).

A possible diagnostic feature of primary remolding is evident as chains of swirled domains caused by initial mixing of the sedi-

ment before emplacement in the pressure tank. Figure 52.13A of sample B-8 shows how the chains are wrapped around the central group of particles. The voids formed by the swirls seem interconnected and might provide a pathway for movement of pore fluids. Figure 52.13B shows an enlarged swirled or bent domain, a primary remolding feature. These disturbance features have been observed in other studies (Bennett et al., 1977; Bohlke and Bennett, 1980). Evidence of mixing or stirring is readily apparent in long chains, but the dominant particle type in this fabric is short chains; thus this type of feature is not obvious or generally apparent in the severely remolded microfabric. Therefore primary remolding effects would be expected to be present in all the ISIMU samples, but subtle. Figure 52.13C of the RAMA sample depicts an *in situ* undisturbed fabric. Notice the straight chain of edge-to-edge domains not influenced by processes involving remolding or probe insertion.

Although the overall fabric of the near-field sample appears slightly denser than the RAMA fabric (Fig. 52.13C) as a result of probe insertion, frequent large void forms (Fig. 52.14A–F) exist that are lined with oriented particles and small domains (≤ 1 µm) arranged stepped face-to-face and end-to-end. These void forms can be thought of as "quasiexpansion" features and appear to be cross sections of microchannels formed by pore fluids moving through the sediment after expansion from ther-
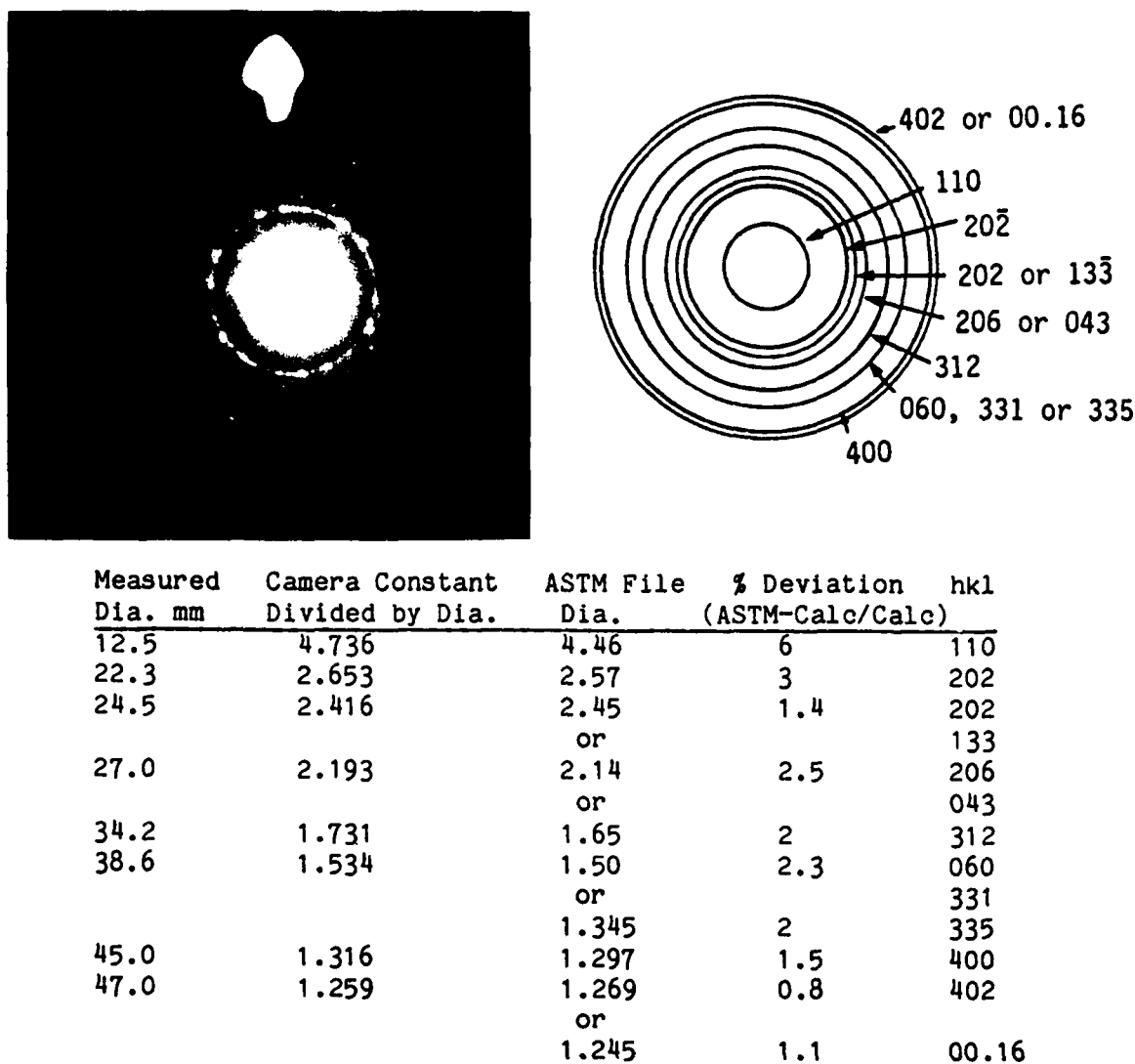
Measured Dia. mm	Camera Constant Divided by Dia.	ASTM File Dia.	% Deviation (ASTM-Calc/Calc)	hkl
12.5	4.736	4.46	6	110
22.3	2.653	2.57	3	202
24.5	2.416	2.45	1.4	202
		or		133
27.0	2.193	2.14	2.5	206
		or		043
34.2	1.731	1.65	2	312
38.6	1.534	1.50	2.3	060
		or		331
		1.345	2	335
45.0	1.316	1.297	1.5	400
47.0	1.259	1.269	0.8	402
		or		
		1.245	1.1	00.16

Figure 52.10. Illite identification using selected area diffraction (SAD). (A) TEM micrograpn of SAD pattern from polycrystalline illite. (B) Drawing of the ring patterns with their Miller indices (*hkl*). (C) Table showing the <6% deviation between the measureᴜ diameters of the unknown sample and the ASTM file values.

mal forces. The pore fluids on heating may transport and push the smallest particles forming the lining of the channels. These conduits are relatively free of small particles, except those too large to be transported, as seen in Figure 52.14B-E. The resin-filled void forms are not to be confused with the white holes in the ultrathin sections (Fig. 52.15A, upper left-hand corner) caused by brittle domains being plucked during microtoming.

An interesting feature more prevalent in the high temperature zones is the appearance of "onion-skin" layering (first described by Brewer, 1964) of stepped face-to-face (Fig. 52.15) particles surrounding the low-density "smectitic" aggregate depicted in Figures 52.15 and 52.16. Cation exchange capacity (CEC) is the measure of a mineral's negative charge being balanced by exchangeable cations. Smectite has a high CEC exemplified by the "onion-skin" layering. Beyond the thin layer of particles lining the smectites are microchannels (Fig. 52.16), important in the transport of pore fluids and small particles. In Figures 52.15B and 52.16B, notice different types of aggregates having the "onion-skin" around them. These predominantly illitic aggregates have a lower CEC, and therefore do not attract small particles of opposite charge. The sediment distribution coefficient (K_d) is the ratio between the sorbed and dissolved metal cations located in sediment pore water (Heath, 1977). Thus increased smectite inhances the barrier effect of the sediment associated with an increased K_d. The aligned smectites exist in the RAMA samples as well, but not to as great an extent (Fig. 52.7).
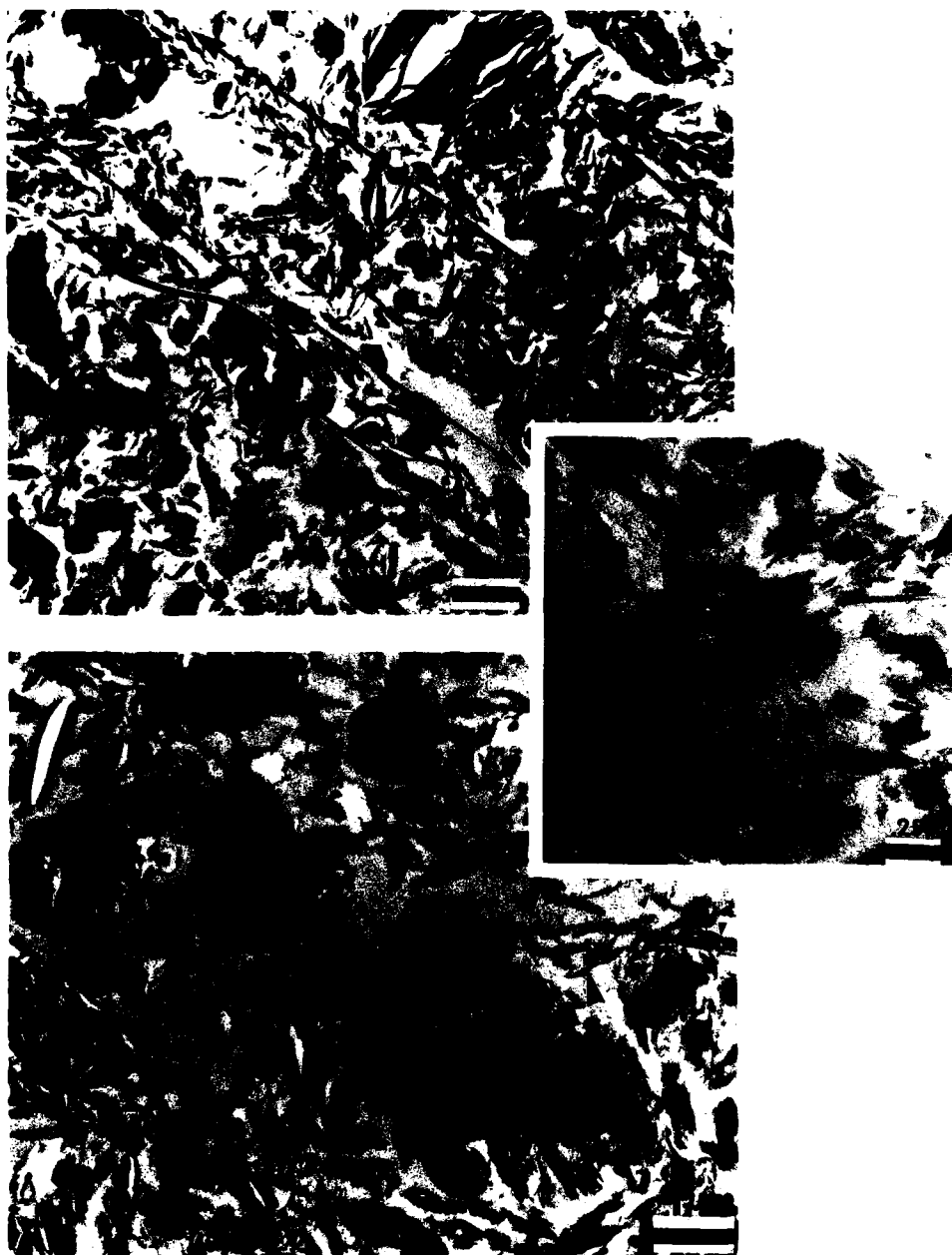
Figure 52.11. Probe insertion disturbance features. (A) Denser arrangement of particles forming broad zones defined by microshear planes in the near-field fabric sample B-8. (B) An enlargement of the microfracture showing ~0.5 μm band of oriented small F-F domains. (C) A microfracture lined by oriented domains (arrows).

Another important aspect of this study was to determine if this remolded, reconstituted, illitic-rich clay sediment is a reasonable material for laboratory study and testing of geotechnical properties. Does it adequately simulate the *in situ* properties and behavior of the red clay deposits? The RAMA mosaic (Fig. 52.7), composed of 20 micrographs representing an area of 2500 μm^2, demonstrates the complexity of the assemblage of clay minerals comprising the fabric. The RAMA mosaic shows the high void ratio fabric typical of Pacific red clays at MPG-1. The prevalent pore spaces of this high porosity fabric are represented by the light-colored background. Figure 52.17 (Bennett et al., 1977) demonstrates models of varying void ratios. RAMA compares to a void ratio of 23.5 (Fig. 52.18) (The heated fabric, described above, looks similar to a medium void ratio of 1.5–2.5). From features in the RAMA mosaic (Fig. 52.7), and Figure 52.18, the sedimentary matrix is dominated by individual particles and small domains behaving as individual particles approximately 1 μm in size. Larger domains (2–5 μm) are fewer in number. This is in contrast to Mississippi-type smectite-rich sediment comprised of domains as the basic framework of the fabric (Bennett et al., 1977). The red clay larger domains are, for the most part, illitic argillites fractured during sectioning with a diamond knife. Figure 52.19A is an enlargement of a subrounded "fractillite" (Bryant and Bennett, 1988) of aeolian origin. The fracture patterns are indicative of the direction of knife motion shown by the arrow. Flexure of these brittle grains during ultrathin sectioning leaves holes (white spaces), but does not affect the integrity of the fabric (Figs. 52.11A, 52.12B, 52.15A, and 52.16B). Elongated or "stringer" fractured illite domains are also common as seen in remolded sample B4 in Figure 52.19B and in the undisturbed RAMA sample. The different appearances of illite are a result of the random deposition orientation of the domains and matrix. Also characteristic of this fabric type is naturally occurring channels providing pathways for pore fluid flow evident in the RAMA mosaic. The channel in Figure 52.7 (upper-left to lower-middle) is 1–2 μm wide and 50 μm long; this is much larger than the cross sections of the microchannels induced from heating (Fig. 52.14).

An array of particle configurations typifies the red clays. Common arrangements include edge-to-edge and edge-to-face particle contacts clearly visible in the RAMA mosaic (Fig. 52.7). Many short chains, predominantly stepped face-to-face and edge-to-edge, are prevalent throughout the fabric, with a lesser amount of longer chains and edge-to-face particle arrangements. Several aggregate types also are common. Sample B4 (Fig. 52.15B) shows a large, subrounded, oriented, low intravoid aggregate. Adjacent is a high intravoid (low density), randomly oriented aggregate of a different mineralogy. This low-density mineral aggregate, probably smectite, has a characteristic small particle (≤ 0.1 μm) size. Smectite is recognized by its "fluffy" appearance (Fig. 52.12B) and is probably authigenic. In aggregate form, the smectitic structural integrity is demonstrated by the lack of tearing or damage common in the fragile ultrathin

Figure 52.12. Disturbance features from probe insertion. (A) Less obvious shear or microfracture (dark lines) identified by chains of stepped F-F small domains. (B) A more easily recognizable microfault lined by oriented domains. The swirled domains (D) are possibly caused by remolding or shearing adjacent to larger argillites (A). The "fluffy," fine particles (inside circle) are perhaps authigenic smectite.

sections. This is due to the high adhesiveness of smectite and the numerous particle contacts. All the mineral aggregates are of a high strength because of the numerous particle contacts and attractive forces at these contacts. Tearing or breakage of the fabric tends to occur between aggregate types, not through them. Chains are also susceptible to breakage, as is evident in the remolded samples. Pusch (1970) observed aggregates moving as units, when subjected to unconfined compression test, and deformation occurring in the connecting links or chains.
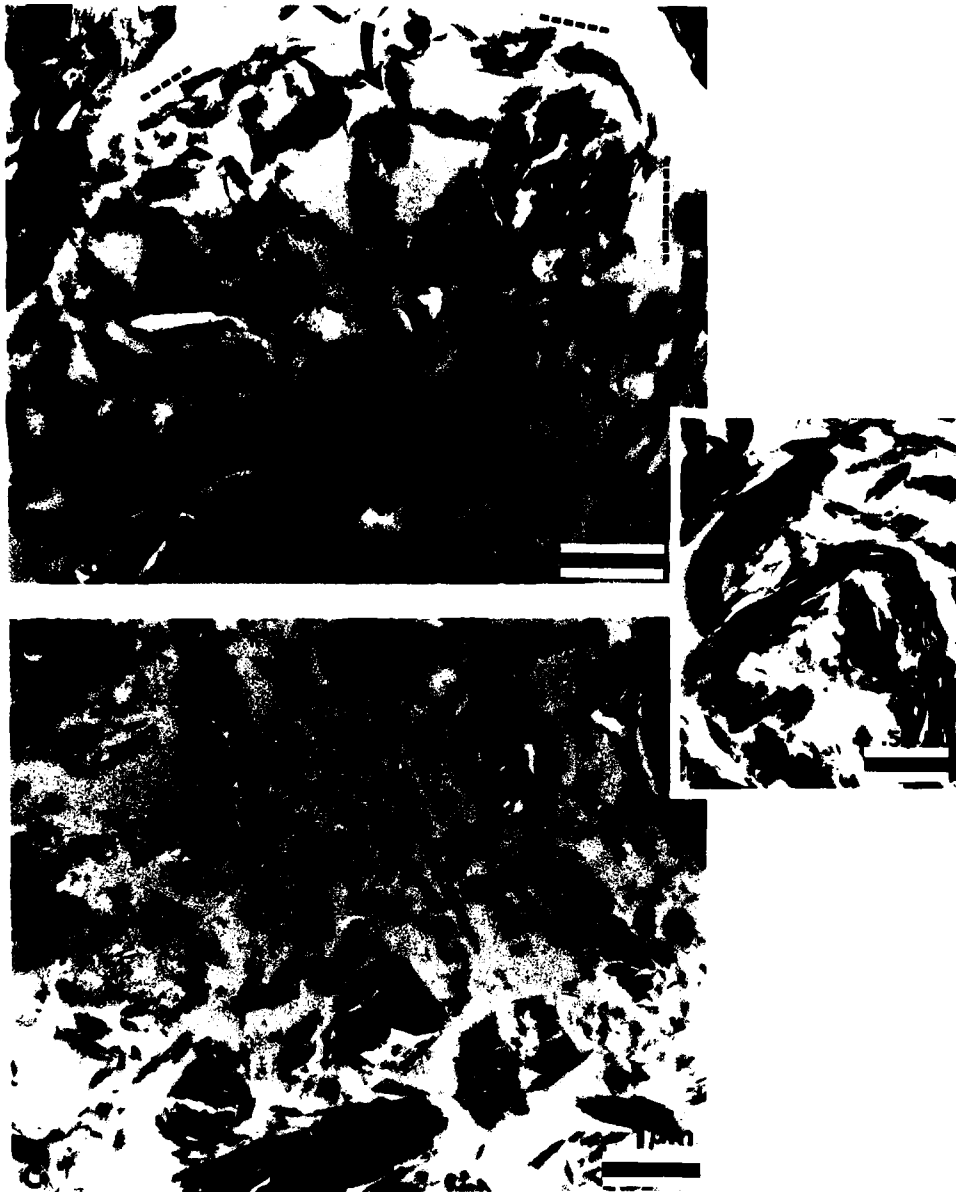
Figure 52.13. (A) Primary remolding causing swirling of domains (arrow) and forming voids performing as pathways (dotted lines) for pore fluids and small particle transport. (B) Enlargement of chain of domains bent, not subjected to remolding or probe insertion stress, demonstrating characteristic straight, long chains of domains (arrow).
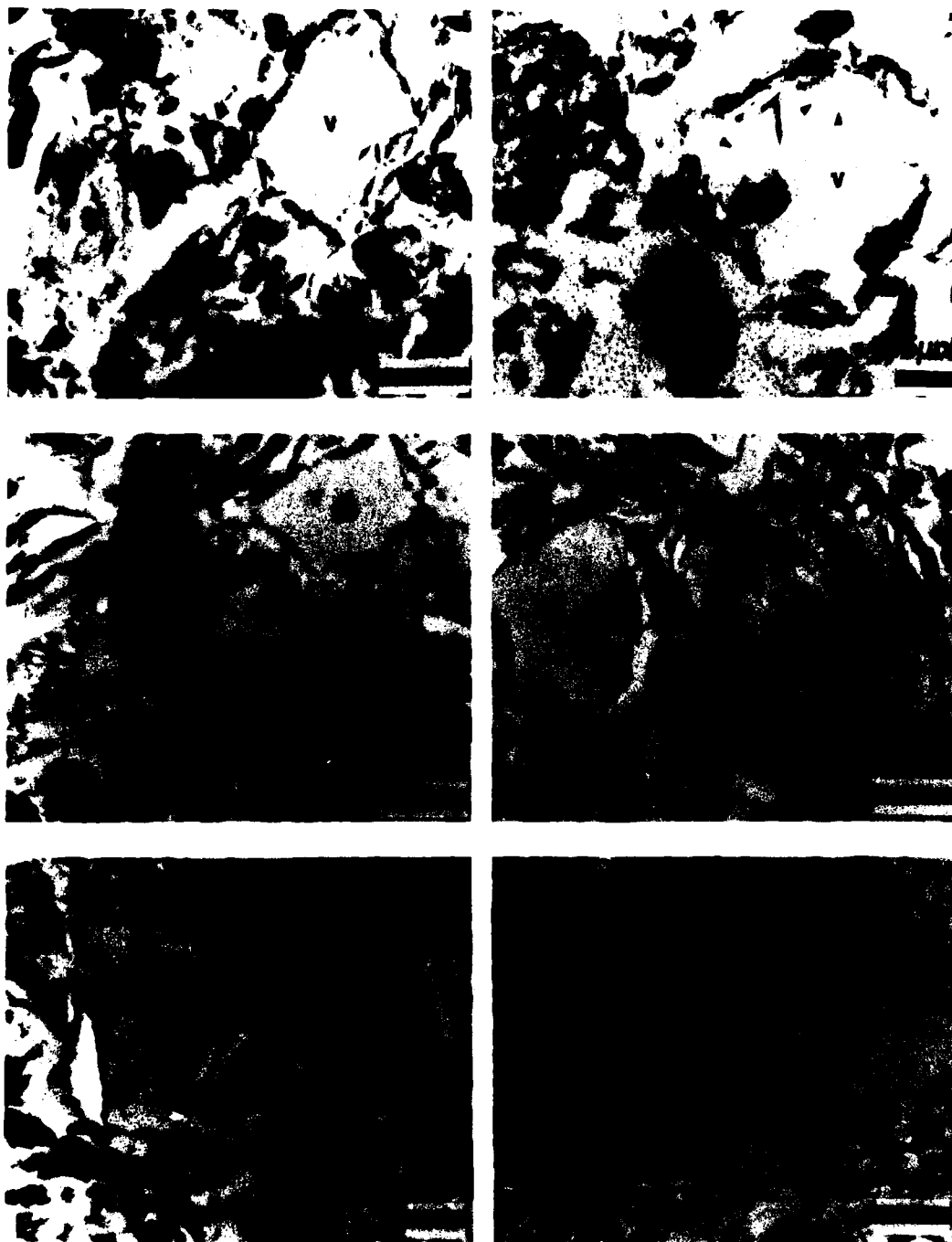
Figure 52.14. Examples of cross-sections of "quasiexpansion" features in near-field samples B-7, B-8, and B-10 which are voids acting as conduits for pore fluids. These voids (V) are lined with E-F and E-E particles and small domains. Micrographs B, C, D, and E show larger particulates which during transport process become trapped within the voids.
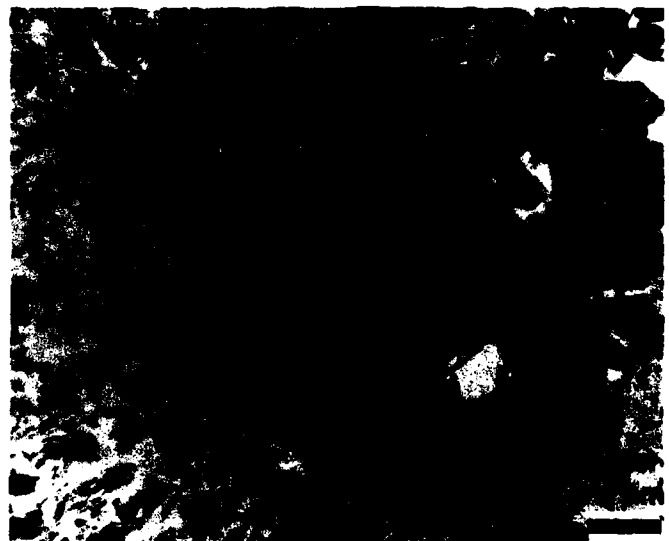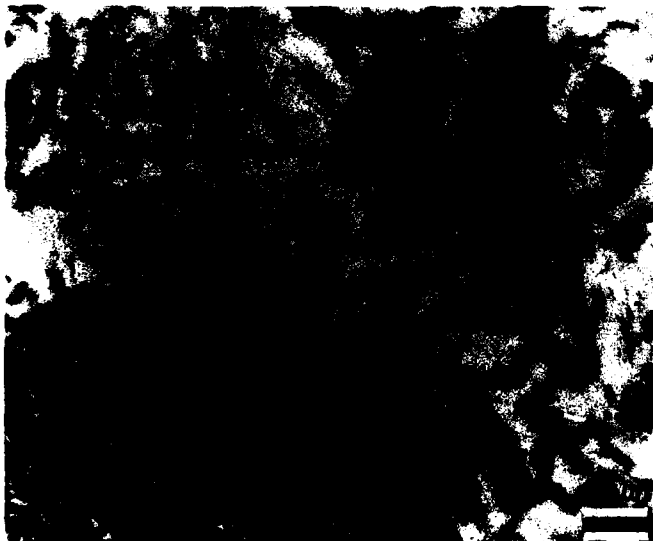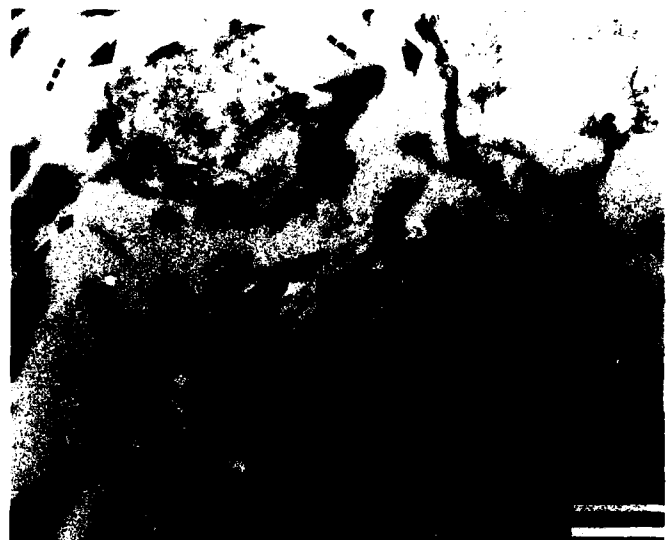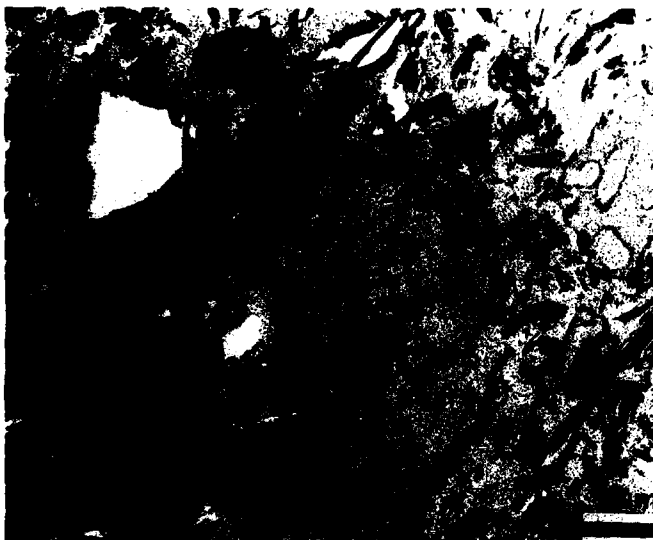
Figure 52.15. (A) Low-density smectite aggregate (S) of sample B-1 demonstrates the "onion-skin" layering of particles typical of heated fabric samples. The tiny dark dots are innocuous contaminates within the embedding resin. In the upper left portion, the micrographs show a hole in the resin as a result of a fractured argillite falling out during ultrathin sectioning. This frequent event does not affect the structural integrity of the fabric. (B) Two aggregate types of contrasting densities (A—high density, S—low density) show the affinity of small domains (arrows) for the high void smectitic aggregates (S).

Figure 52.16. (A) Sample B-3 shows a low-density aggregate, probably smectite (S), surrounded by "onion-skin" layering of E-E and E-F particles (arrows), beyond which are channels (dotted line) for pore fluid transport. (B) Small particles and domains line the low density aggregate (S). Other aggregate types (A) have relatively few particles adhering to their surfaces.

Conclusions

Clay fabric was the foci for assessing the effects of thermal exposure and mechanical disturbances on this illitic sediment as a result of probe insertion, remolding, and varying temperature fields induced during ISIMU. In response to heating, several physical property parameters varied; shear strength increased and water content decreased. A localized transformation of the clay mineralogy from illite to smectite in the "baked zone," subjected to high temperatures, relates to an increase in the pore fluid potassium levels associated with its release from the interlayer of illite.

Fabric analysis did show some sediment response from primary remolding during reconstitution of the sediment before the ISIMU experiment. This was evidenced by the swirling, twisting, and breakage of longer chains of domains. Secondary remolding and traction stress caused by mechanical disturbance induced by probe insertion resulted in localized compression features in the near-field samples, demonstrated by an increase
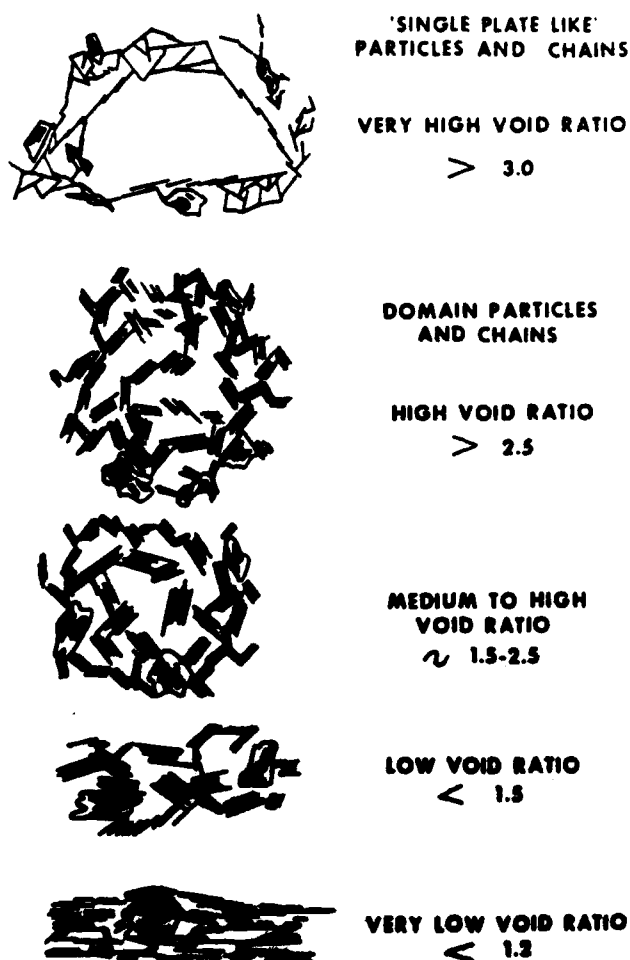
'SINGLE PLATE LIKE'
PARTICLES AND CHAINS

VERY HIGH VOID RATIO

> 3.0

DOMAIN PARTICLES
AND CHAINS

HIGH VOID RATIO

> 2.5

MEDIUM TO HIGH
VOID RATIO

$\sim$ 1.5-2.5

LOW VOID RATIO

< 1.5

VERY LOW VOID RATIO

< 1.3

Figure 52.17. Clay fabric models for submarine sediments (Bennett et al., 1977).

Figure 52.18. High void ratio "undisturbed" fabric of *in situ* RAMA sample showing microchannels (dotted line). The matrix is predominantly of particles and small domains (p) arranged stepped F-F and E-E, and forming short chains (arrows). (A) Notice the microchannels for fluid transport. (B) Numerous large argillite domains (L) exist which fracture during ultrathin sectioning.

in fabric density and alignment of broad bands of particles. The RAMA sample, the control not subjected to remolding or laboratory reconstituting effects, displayed longer, straighter chains of particles forming a less dense fabric.

Thermal forces resulted in "quasiexpansion" features defined as small particle-lined voids created by heated pore fluid moving through the sediment and pushing small particles aside forming the channel walls. The movement of fluids also brought small particles into contact with the smectitic-appearing aggregates bearing a large CEC, and this resulted in increased layers of stepped, face-to-face particles adhering to the aggregates in the near-field, remolded samples. Smectitic aggregates in the RAMA samples had decreased amounts of "onion-skin lining" of particles, as seen in the TEM micrographs.

The complexity of this Pacific red clay fabric type is striking, as seen by the many types of particles, such as large 2-5 μm argillite domains, aggregates of varying densities, and the channels for fluid movement approximately 2 μm in width. Various

arrangements of particle contacts are observed, including edge-to-edge, stepped face-to-face, and lesser amounts of edge-to-face arrangements. The dominant particles comprising the matrix are small domains ~ 1 μm in length. The *in situ* orientation of particles comprising the fabric is random and forms a high void ratio sediment. The grain size of the far-field samples varies little from the nonremolded control.

Pacific illitic-rich red clay appears to be an excellent material for laboratory use and comparative geotechnical studies of *in situ* properties of sediment responses. This is evident by the remarkable similarity of the microfabric features between the Pacific illitic-rich red clay and the same sediment-type subjected to the stress of mechanical disturbance and heating. The
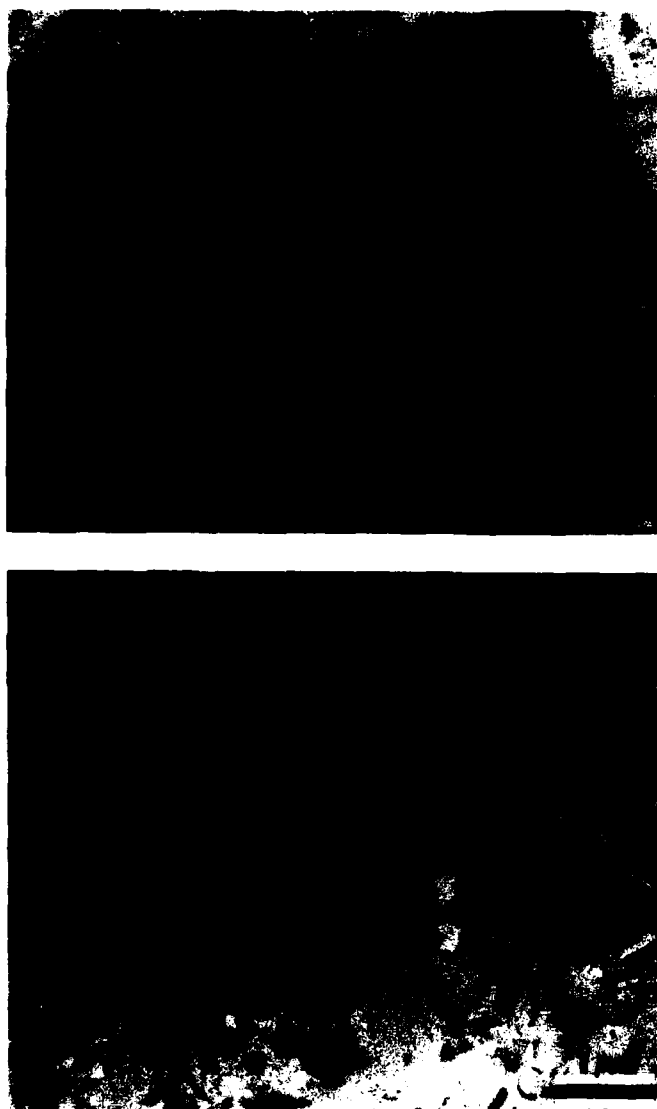
Figure 52.19. (A) A large subrounded argillite (FA) indicative of eolian origin. The fracture pattern is normal to the direction of sectioning (dark line) with diamond knife. (B) Characteristic fractured large "stringer" argillites (st) commonly found.

dominant particle type exemplified by the ≤ 1 μm matrix of domains and short chains is the single most important characteristic that makes this a resilient and durable material for both *in situ* and laboratory use. It is the microstructure, in addition to grain size and mineralogy, which controls the response and the physical properties including porosity, permeability, isotropy, and anisotropy of the sediment.

The role of microfabric of the Pacific illitic red clay sediment to radioactive waste disposal is summarized below. This provides an excellent example of how fabric studies can address practical problems and furnishes insight into engineering applications:

1. Enhanced geotechnical properties such as a residual shear strength, lower porosities, and permeabilities in the plastic zone positively impact the predictive capability of waste-containing canisters.
2. Although remolding features were observed such as swirled chains of particles and bent domains, no microfabric or grain size changes, which significantly affected the bulk physical properties, occurred in spite of the severe remolding in the laboratory.
3. Although small-scale microshears and localized orientation of particles in the direction of stress occurred, no significant fabric changes were observed in the zone of plastic deformation as predicted by theory.
4. Enhanced positive mineralogical changes ensue by enhanced K_d from the transformation of illite to smectite. The larger the coefficient, the better the radionuclide cation is contained in the sediment because of increased isolation capacity of the sediment.
5. No significant fabric changes due to thermal changes up to 296°C.
6. The gross nature and appearance of the undisturbed sediment compared to the remolded sediment are strikingly similar. The Pacific red clay is virtually an isotropic sediment, as evidenced by its microfabric.

Acknowledgments

References

Andrews KW, D.J. Dyson, and S.R. Keown, 1971. Interpretation of Electron Diffraction Patterns. Plenum Press, New York, 239 p.

Bennett, R.H., 1976. Clay fabric and geotechnical properties in selected submarine sediment cores from the Mississippi Delta. Ph.D. dissertation, Texas A&M University, College Station, TX, 269 p.

Bennett, R.H., W.R. Bryant, and G.H. Keller, 1977. Clay fabric and geotechnical properties of selected submarine sediment cores from the Mississippi Delta. NOAA Professional Paper No. 9, 86 p.

Bohlke, B.M., and R.H. Bennett, 1980. Mississippi prodelta crusts: a clay fabric and geotechnical analysis, Marine Geotechnology, v. 4, p. 5–82.

Brewer, R., 1964. Fabric and Mineral Analysis of Soils. Wiley, New York, 470 p.

Bryant, W.R., and R.H. Bennett, 1988. Origin, physical, and mineralogical nature of red clays: the Pacific Ocean basin as a model. Geo-Marine Letters, v. 8(4), p. 189–249.

Burkett, P.J., 1987. Significance of the microstructure of Pacific red clays to nuclear waste disposal. M.S. thesis, Texas A&M University, College Station, TX, 79 p.

Folk, R.L., and W.C. Ward, 1957. Brazos River Bar: a study in the significance of grain size parameters. Journal of Sedimentary Petrology, v. 27, p. 3–27.

Harvard, M.E., and G.W. Brindley, 1964. Swelling properties of synthetic smectites in relation to lattice substitutions. Clays and Clay Minerals, v. 13, p. 209–222.

Heath, G.R., 1877. Barriers to radioactive waste migration. Oceanus, v. 20(1), p. 26–30.

Hollister, C.D., D.R. Anderson, and G.R. Heath, 1981. Subseabed disposal of nuclear waste. Science, v. 213, p. 1321–1326.

Index to Powder Diffraction File, 1969. American Society for Testing and Materials, Philadelphia, PA, p. 1385.

International Atomic Energy Agency, IAEA Inf. Circ. 205/Add.1/Rev. 1, 1978, 1972 Convention on the Prevention of Marine Pollution by Dumping of Wastes and Other Matter, 26 U.S.T. 2403, TIAS No. 8165, entered into force 1975, reprinted in 11 Int. Leg. Mat., 1292 (1972); D.A. Deese, Nuclear Power and Radioactive Waste (Health, Lexington, MA, 1978), p. 65–67.

Jackson, M.L., 1969. Soil Chemical Analysis Course, 2nd ed., 8th printing. Department of Soil Science, University of Wisconsin, Madison, WI, 895 p.

Lambe, T.W., 1951. Soil Testing for Engineers. Wiley, New York, 165 p.

McTigue, D.F., J. Lipkin, and R.H. Bennett, 1986. Consolidation under an isotropic total stress increase: part I, analysis for compressible constituents, Geotechnique, v. 36(1), p. 1–9.

Miller, J.B., V.W. Miller, and L.O. Olson, 1982. ISHTE Simulation APL-UW engineering report, University of Washington, Seattle, WA, 83 p.

Noll, W., 1930. Syntheses von Montmorilloniten. Chem. Erde., v. 10, p. 129–154.

Olson, L.O., and J.G. Harrison, 1979. Sea floor system for an *In Situ* Heat Transfer Experiment, Proceedings, OCEANS '79, IEEE Pub. 78 Ch 14 78-7 OEC, p. 421–423.

Percival, C.M., 1982. Laboratory simulation for a deep-ocean *In Situ* Heat Transfer Experiment, OCEANS '82, MTS/IEEE Conference Record, Sept. 20–22, Washington, DC, 6 p.

Percival, C.M., 1983. The Subseabed Disposal Program — *In Situ* Heat Transfer Experiment (ISHTE), SAND80-0202, Sandia National Laboratories, Albuquerque, NM, 47 p.

Percival, C.M., D.F. McVey, L.O. Olson, and A.J. Silva, 1980. *In Situ* Heat Transfer Experiment (ISHTE), OCEANS '80 NTS/IEEE Conference Record, Sept. 20–22, Washington, DC, p. 567–573.

Percival, C.M., L.O. Olson, R.H. Bennett, F.L. Sayles, and A.J. Silva, 1987. The Subseabed Disposal Program *In Situ* Heat Transfer Experiment (ISHTE) final design report. SAND86-2008-UC-70, Sandia National Laboratories, Albuquerque, NM., 104 p.

Pusch, R., 1970. Microstructural changes in soft quick clay at failure. Canadian Geotechnical Journal, v. 7, p. 1–7.

Sedleski, I.D., 1937. Genesis of minerals from soil colloids of the montmorillonite group. C.R. Academy of Science, U.S.S.R., v. 17, p. 375–377.

Seyfried, W.E., Jr., and J.L. Bischoff, 1981. Experimental seawater-basalt interaction at 300°C, 500 bars, chemical exchange, secondary mineral formation and implications for the transport of heavy metals: Geochemica Cosmochimica Acta, v. 45, p. 135–147.

Silva, A.J., and S.A. Jordan, 1984. Consolidation properties and stress history of some deep sea sediments. In: Denness, B. (ed.), Seabed Mechanics. Graham & Trotman, London, p. 25–39.

Thorton, E.C., 1983. Experimental and theoretical modeling of sediment-seawater hydrothermal interactions at constant temperature and in a thermal gradient: implication for the diagenesis and metamorphism of marine clay and the subseabed disposal of nuclear waste. Ph.D. dissertation, University of Minnesota, 193 p.

Veblen, D.R., 1986. Transmission electron microscopy: scattering processes, conventional TEM, and high-resolution imaging. In: Electron Microscopy and Microprobe Techniques in Clay Mineral Analysis Workshop, Clay Minerals Society Annual Meeting, Jackson, MS, 42 p.